Received: 13 June 2023 | Revised: 23 January 2024 | Accepted: 26 January 2024

DOI: 10.1002/suco.202300469

ARTICLE

fib CEB-FIP WILEY

Enhancement of impact resistance of alkali-activated slag concrete through biochar supplementation

Harshani Egodagamage[1,2] | **Hiran Yapa**[2] | **Samith Buddika**[2] | **Thomas Loh**[1] | **Satheeskumar Navaratnam**[1] | **Yulin Patrisia**[1] | **Kate Nguyen**[1]

[1]School of Engineering, RMIT University, Melbourne, Australia

[2]Faculty of Engineering, University of Peradeniya, Peradeniya, Sri Lanka

Correspondence
Kate Nguyen, School of Engineering, RMIT University, 124 La Trobe Street, Melbourne, VIC 3000, Australia.
Email: kate.nguyen@rmit.edu.au

Abstract

Biochar is a well-known sustainable and effective additive used in mortar/concrete to improve its mechanical properties. However, its potential to improve the impact resistance of concrete is still unexplored. This paper investigates biochar's effectiveness in improving the strength and impact performance of alkali-activated slag concrete (AASC). Five AASC samples with 0%, 2%, 4%, 6%, and 8% rice husk biochar (RB) were employed in an experimental program. The strength and the impact resistance were tested, and the latter was assessed over a drop-weight test conforming to the ACI Committee 544 guidelines. The crack propagation of the impact-tested samples was examined using micro-CT images. The results showed that adding RB up to 6% improved, notably the 28-day compressive strength of AASC. At 6% RB, the strength enhancement was 44.6%, whereas no additional gain was observed at the 8% RB blend. More importantly, except for the 8% RB sample, the impact resistance was considerably augmented with the RB level increment. The increment in the impact number at the first crack and the failure in the 6% RB sample were as high as 185% and 180%, respectively. The reduction in the solution/binder ratio of the mix with the addition of biochar and the internal curing effect of biochar were deemed to be responsible for these improvements. However, possibly due to biochar's brittle characteristics, the increase in RB dosage from 6% to 8% reduced the impact resistance drastically.

KEYWORDS

alkali-activated slag concrete, compressive strength, impact resistance, Rice husk biochar

1 | INTRODUCTION

Ordinary Portland cement (OPC) is the commonly used cementitious material in the construction industry. However, the need for alternative binders emerges highly due to higher CO_2 emissions and energy consumption related to OPC production.[1] Over the recent past, alkali-activated materials have attracted reasonable attention as green alternatives to OPC due to their less CO_2 emission and less requirement of natural resources.[1,2] For instance, Yang

et al.[3] revealed that despite the fact that the CO_2 reduction rate of alkali-activated concrete depends on the type, concentration, and dosage of the alkaline activators, it reduces the CO_2 emission by about 55%–75% as opposed to OPC concrete. In addition, alkali-activated slag (AAS) is well known for its ability to achieve outstanding mechanical performance at ambient curing conditions.[2]

Alkali-activated slag concrete (AASC) is produced through the chemical reaction between ground-granulated blast furnace slag (GGBS) and an alkaline activator. GGBS is a by-product of pig iron manufacturing, and it is estimated that the global annual production of GGBS is to be 270–320 Mt.[1] Moreover, the energy consumption (1300 MJ) and the CO_2 emissions (0.07 t) related to the production of one ton of GGBS are very less in comparison to those in OPC production.[1] The selection of an appropriate alkaline activator is crucial as it critically affects the carbon footprint and mechanical properties of the final product. The most frequently used alkaline activator in AAS production is a combination of alkaline hydroxides and silicates (e.g., sodium hydroxide and sodium silicate) to achieve a high degree of alkali activation.[2,4] However, these activators, particularly sodium silicate, are highly carbon-intensive and expensive materials in AAS composites.[2] Furthermore, AAS activated by sodium silicate is difficult to handle due to its reduced workability and quick setting.[5,6] Therefore, the selection of user- and environmental-friendly alkaline activators is much needed for the future development of AAS.

Recent studies have successfully attempted to activate GGBS with sodium carbonate (Na_2CO_3) with the aim of producing AAS with a low carbon footprint and improved performance in terms of workability and shrinkage. However, the low initial strength developed at ambient curing has discouraged the use of Na_2CO_3 as an alkaline activator in AAS production.[1,4,6] Zhang et al.[6] found that activation of slag (with $D_{50} = 8.1$ μm) by sodium carbonate (4% sodium oxide equivalent) yielded a very low 3-day compressive strength of 0.8 MPa, while the strength increased up to 29.7 MPa at the age of 28 days. As a solution, both Zhang[6] and Rashad[7] proposed to increase the slag fineness. Rashad et al.[7] reported an increment in 3-day and 28-day compressive strength by 137.4% and 51.7%, respectively, when the slag fineness was increased from 2500 to 5000 cm^2/g. Similarly, Tan[8] provided evidence that wet ultra-fine slag ($D_{50} = 3.87$ μm) could be activated efficiently by weak bases such as sodium sulfate and sodium carbonate at room temperature. Supplementation of additives to accelerate the reaction rate is another method proposed in the literature. Gao et al.[4] reported an increment in 1-day compressive strength up to 21.8 MPa due to the addition of calcium carbide residue to the Na_2CO_3-activated slag. Moreover, Jiao[5] discovered that supplementing NaOH at a Na_2CO_3: NaOH molar ratio of 15:10 along with a Na_2O content of 6% could achieve a 3-day compressive strength of around 45 MPa. A similar combination of Na_2CO_3 and NaOH was used in the authors' previous study as well and yielded a 3-day compressive strength of 22.4 MPa.[9]

Biochar is a well-known CO_2 adsorbent material in cementitious applications due to its ability to capture and sequester CO_2.[10] Gupta[11] revealed that the CO_2 adsorption capacity of mixed wood sawdust biochar was as high as 1.67 mmol/g of biochar. Thus, the addition of 2 wt.% biochar in cementitious mortar was reported to reduce the net global warming capacity by 15.3%. Similarly, it has been reported that peanut hull biochar has a CO_2 adsorption capacity of 0.86 mmol/g.[12] Moreover, Praneeth[13] discovered that the incorporation of 2–6 wt.% of corn stover biochar enhanced CO_2 uptake in the cement-fly ash blocks. Meanwhile, numerous studies reported that the compressive strength of cementitious composites improved with the supplementation of biochar. Gupta and Kua[14] observed an increase in both the 1-day and 28-day compressive strength of cementitious mortar by 20%–25% due to the addition of 0.5%–1% of mixed wood sawdust biochar. Praneeth[13] reported an improvement in the 28-day compressive strength of OPC mortar from 38 MPa to 40.6 MPa when the corn stover biochar content was increased from 0% to 6%. However, further increments in biochar dosage from 6% to 8% reduced the compressive strength. Zeidabadi[15] observed an increase in the 28-day compressive strength of cementitious concrete by 20.4% with the addition of 5% rice husk biochar, and increasing biochar content up to 10% reduced the compressive strength. Furthermore, the authors' previous study revealed that the increment of biochar replacement level from 1% to 5% in AAS mortar improved the 28-day compressive strength by 5.9%.[9] It has been discussed in the literature that the high-water absorption and retention properties of biochar are mainly responsible for these compressive strength improvements. For instance, porous biochar reduces the effective water-to-binder ratio (w/b) of the mix as it absorbs a portion of the mixing water, lowering the evaporable free water content of the mix, which can create capillary pores and densify the microstructure.[11,16] Moreover, a part of the absorbed water is retained by biochar, which then emerges as an internal curing agent.[10,17] Consequently, the hydration efficiency is increased.[10,17] Enhanced formation of the hydration products also leads to densifying the microstructure.[9]

Depending on the intended application and properties of biochar, the feedstock and pyrolysis conditions need to be selected. It has been discovered that a low heating rate (10°C/min) enhances the micropore fraction of biochar, which is favorable for carbon sequestration.[11,18,19] This is

due to the fact that the low heating rate smoothens the release of volatiles and organics. Also, the application of a sufficient residence time (generally in the range of 30–120 min) accelerates the release of volatiles and enhances the pore volume of biochar.[18] However, very long residence times consume more energy. Moreover, Chen[20] found that sewage sludge biochar produced at a residual time of 60 min performed well in mortar in comparison to that produced at residual times of 30, 120, and 180 min. Furthermore, the yield of biochar is considered to be high when slow pyrolysis is adopted.[19] In addition, biochar's flammability is also reduced.[19]

The impact resistance of concrete is an essential engineering parameter, especially for the structures being designed to resist the impact loads (e.g., road barriers and rock fall protection walls). Previous researchers have discovered different methods of improving the impact resistance of OPC concrete. The addition of steel fibers is reported to enhance the impact resistance of concrete considerably, as the pullout of those fibers can absorb a large quantity of the impact energy during a collision.[21,22] In addition, long steel fibers are more efficient at restricting the growth of micro cracks.[21] Kangning et al.[23] found that replacing river sand (between 0.6 and 1.25 mm) with porous pottery sand could improve the impact energy required for the first crack by 133%. The reason behind this improvement is the energy absorption capacity of the porous pottery sand. However, the influence of the water absorption of the pottery sand toward the mechanical properties still needs to be explored. Microstructure densification is another method for enhancing the impact resistance of concrete. It has been reported in previous studies that the addition of supplementary materials such as silica fume, which densifies the microstructure, could increase the impact resistance of concrete. Gupta et al.[24] observed that the addition of 0%, 5%, and 10% silica fume to OPC concrete increased the number of impacts (in the drop hammer impact test) required for the failure from 65 to 67 and 72, respectively. Similarly, Nili et al.[25] reported that the 8% cement replacement by silica fume improved the number of such impacts at the first crack and the failure by 6.9 times and 6.5 times, respectively. Moreover, Ameri et al.[26] found that replacing natural sand in OPC concrete with 20%, 40%, and 60% of copper slag increased the impact energy at the initial crack level by 13%, 25%, and 42%, respectively, in contrast to the control mix. Similarly, the impact energy at the failure was increased by 14%, 31%, and 50%, respectively. This increment in impact resistance was attributed to the denser microstructure resulting from the incorporation of CS. In this light, biochar could also improve the impact resistance of concrete since it could potentially densify the microstructure of concrete.[15,20,27–29] However, such a hypothesis has yet to be confirmed through experimental tests.

Even though many studies have been conducted on the impact resistance of OPC concrete, limited studies are found to be focused on the impact behavior of AASC and on methods of improving its impact resistance. Nis et al.[30] investigated the effect of the inclusion of nanosilica and steel fibers on the impact resistance of AASC and discovered that the incorporation of 2% nanosilica and 1% long steel fibers enhanced the impact energy by 144.5 times compared to the control specimens. Similarly, Xu[31] examined the effect of the length and dosage of the polypropylene fiber on the impact resistance of AAS mortar and revealed that the increase in fiber length and dosage improved the energy absorption capacity. Accordingly, 0.2% of the 15-mm length polypropylene fibers yielded the highest impact resistance of the AAS mortar. Abubakr et al.[32] studied the effect of silicate modulus and sodium oxide dosage on the impact performance of AAS mixes. They found that increasing the sodium oxide content from 6% to 8% at a silica modulus of 1.5 enhanced the impact energy absorption by 107%. In addition, it was concluded that AAS mixtures showed better impact absorption compared to cement-based materials. Based on these facts, it is of interest to study the impact performance of biochar-supplemented AASC. In this context, the current study was formulated to study the influence of the blending of biochar on the impact resistance of the AASC and to determine the best blending level of biochar in the AASC in terms of impact and strength performances.

The drop hammer impact test based on ACI 544 committee[33] is widely used to determine the impact resistance of concrete because of the simplicity of the approach.[25,34,35] Therefore, this study aimed at testing five different AASC mixes with various biochar levels (0%, 2%, 4%, 6%, and 8%) under that particular drop hammer impact test method. The study was further extended to evaluate the biochar's influence on the microstructure and crack propagation of AASC using SEM analysis and micro-CT scanning. In addition, the effect of biochar on the slump flow and the compressive strength was monitored. The research methodology is illustrated in Figure 1.

2 | MATERIALS AND METHODS

2.1 | Materials

2.1.1 | GGBS, alkaline activators and aggregates

The main alkali-activated binder used in this study was GGBS, which was collected from Siam City Cement

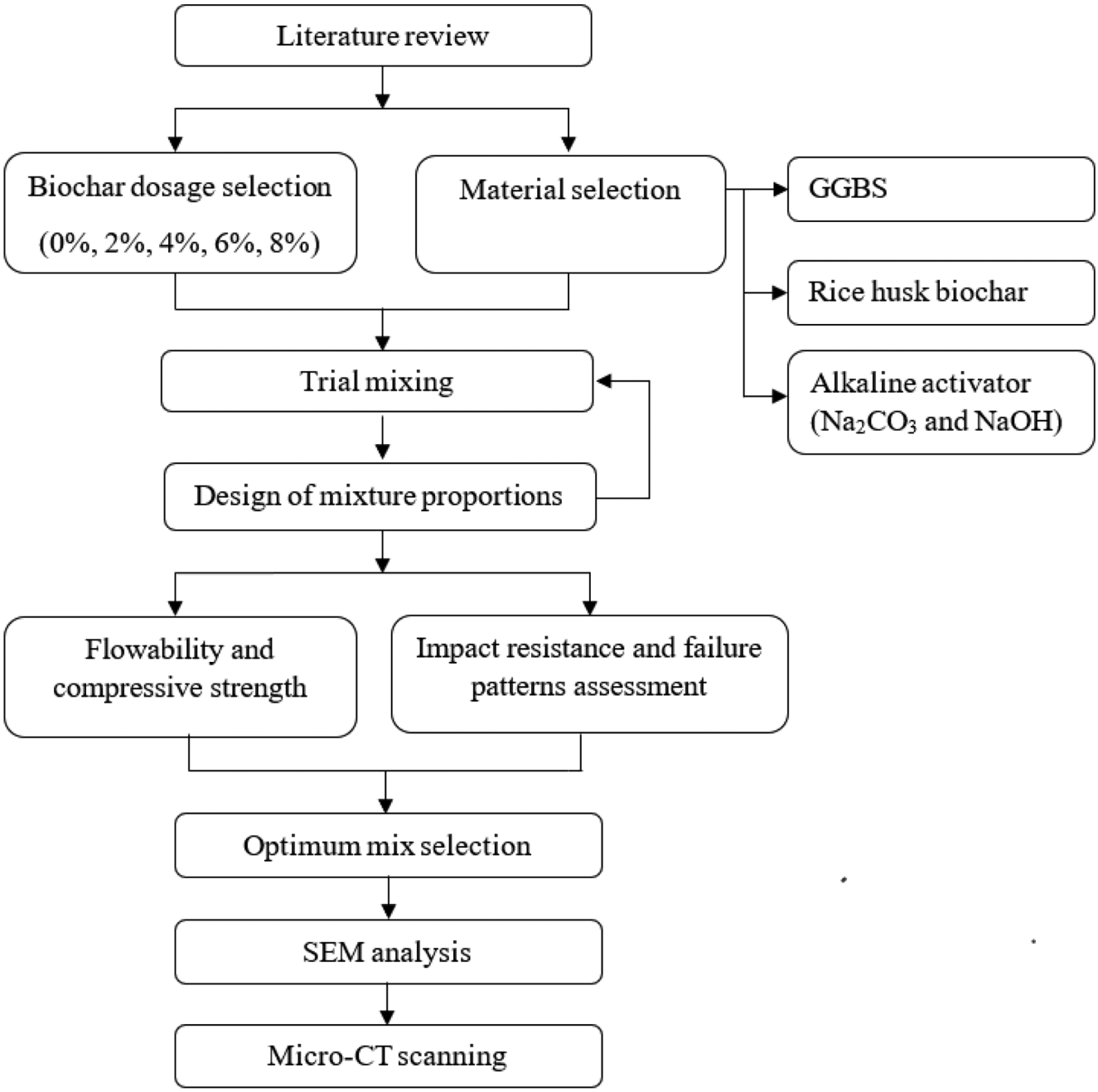

FIGURE 1 Research methodology.

TABLE 1 Chemical composition of GGBS (%).

Oxide	CaO	SiO_2	Al_2O_3	MgO	Fe_2O_3	K_2O	Na_2O	SO_3	MnO	P_2O_5	LOI
Percentage (%)	40.39	35.35	12.19	6.18	0.75	0.3	1.09	0.1	0.13	0.05	1.4

(Lanka) Limited. The unground GGBS was processed using a laboratory ball mill that was operated at a speed of 36 rpm in order to increase the fineness. The production rate of the GGBS powder was 5 kg per 16 h. A laser diffraction particle size analyzer determined that the median particle size (D_{50}) of the ground slag was 6 μm. The specific gravity of the slag was measured to be 2.9. LOI was measured by heating GGBS in a muffle furnace at a temperature of 950°C for a maximum period of 1 h. Table 1 outlines the chemical composition of the GGBS that was assessed using X-ray fluorescence (XRF) spectrometry. The alkaline activator was prepared by

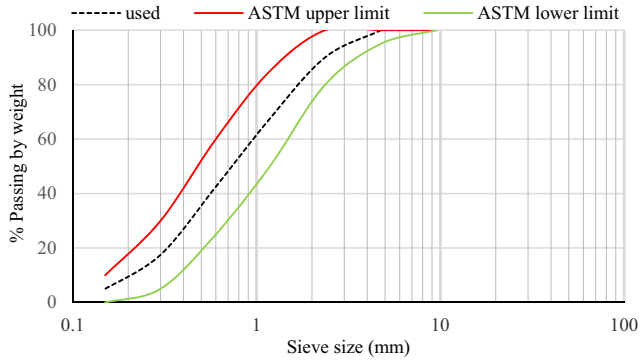

FIGURE 2 Particle size distribution of fine aggregates.

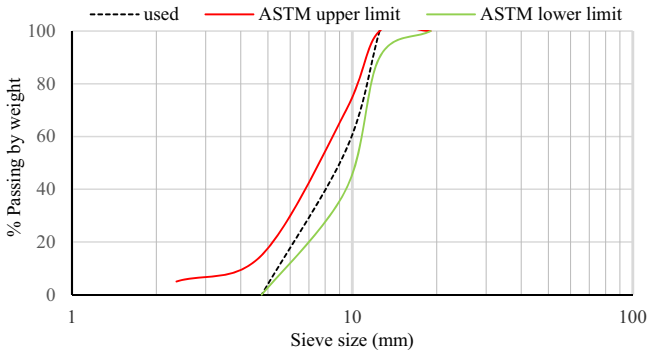

FIGURE 3 Particle size distribution of coarse aggregates.

combining analytical grades of NaOH pellets (98.5%–100.5% purity) and Na_2CO_3 (99.9% purity). The coarse aggregate was used in the saturated, surface-dry conditions. It was achieved by submerging the aggregate in water for a continuous 3-day period until all the particles were saturated, and the excess water was drained afterward.[36] The aggregate was then gently surface dried using dry clothes and dried in the air until all the visible films of water were removed. The maximum size and the specific gravity of the coarse aggregate were 12 mm and 2.75, respectively. Natural river sand with a specific gravity of 2.65 was used as the fine aggregate. Grading coarse and fine aggregates was done as per ASTM C33[37] and the particle size distribution curves (along with upper and lower grading limits) are illustrated in Figures 2 and 3.

2.1.2 | Biochar

Biochar was prepared from rice husk (Figure 4) collected from Sri Lanka. The rice husk was washed fully with water to remove any impurities and oven-dried at 80°C for 48 h (until getting a constant mass) before subjecting it to pyrolysis.[38] Fully filled crucibles with rice husk were sealed such that the air inside the crucible was minimal

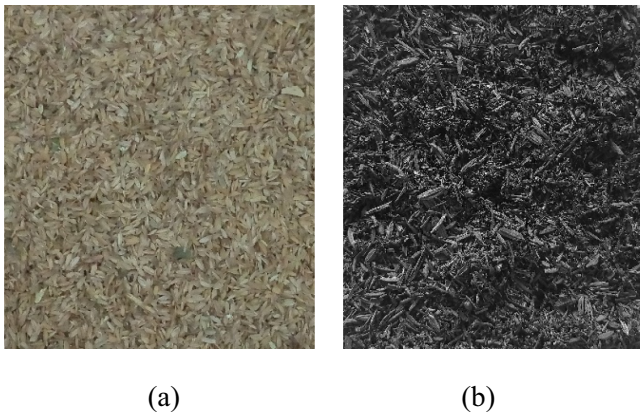

FIGURE 4 Images of: (a) rice husk before pyrolysis; (b) rice husk after pyrolysis (RB).

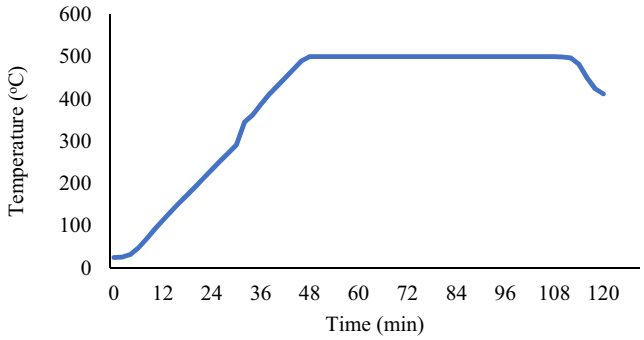

FIGURE 5 Pyrolysis temperature profile.

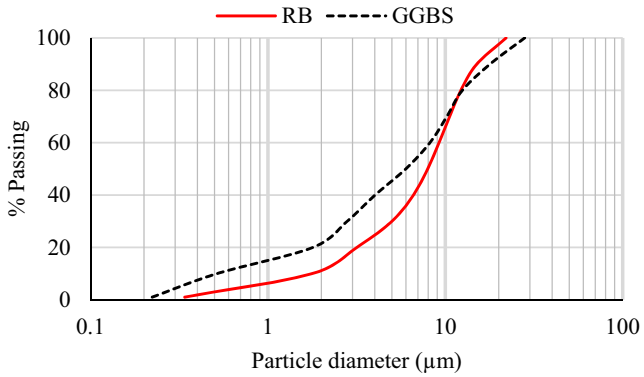

FIGURE 6 Particle size distribution of RB and GGBS.

and placed inside a Yamato FO-310 muffle furnace.[20,39] The pyrolysis was carried out at 500°C. The selection of the biochar type and the pyrolysis temperature was based on the authors' previous study.[9] The furnace was heated up to 500°C at a heating rate of 10°C/min, and after that, the temperature was maintained for 60 min (Figure 5). Hereafter, the biochar produced after rice husk pyrolysis is designated as RB. The RB was stored in a sealed container until the time of mixing.

Before mixing with GGBS, biochar was ground using a ball mill and sieved through a 75-μm sieve. A laser diffraction particle size analyzer determined the median particle size of biochar (D_{50}) to be 7.9 μm. The particle size range of RB used in this study was between 0.34 and 22.3 μm. The particle size distribution of RB (and GGBS) is illustrated in Figure 6.

2.2 | Characterization of biochar

2.2.1 | Morphology

Figure 7 shows the morphology of RB that was determined by the scanning electron microscope. The rough texture of RB, along with the inherited surface protrusions from the feedstock, is shown in Figure 7a. The highlighted area in Figure 7b illustrates the cellular structure of RB, which might have been inherited from the parent biomass or created because of the release of organics and volatiles during the pyrolysis.

2.2.2 | pH and absorption

The pH of RB was determined by mixing biochar and distilled water at a weight proportion of 1:10. Then, the solution was thoroughly mixed for 30 min and stabilized for 1 h before measuring the pH using a pH meter.[40,41] The pH value was found to be 8.02, indicating the basic nature of RB.

The "tea bag method" was used to calculate the absorption capacity of RB in water and the extracted pore solution of AAS (EPS-AAS).[16,28,42] The measurement of the water absorption capacity of RB was as follows: A 5 g of RB was placed inside an empty tea bag, and it was fully submerged in water. Alongside, an empty tea bag was immersed to find out the amount of water absorbed by biochar only. The water intake was measured at regular time intervals until there was no difference in mass. A similar procedure was adopted to determine the absorption of RB in EPS-AAS; thus, RB was fully submerged in

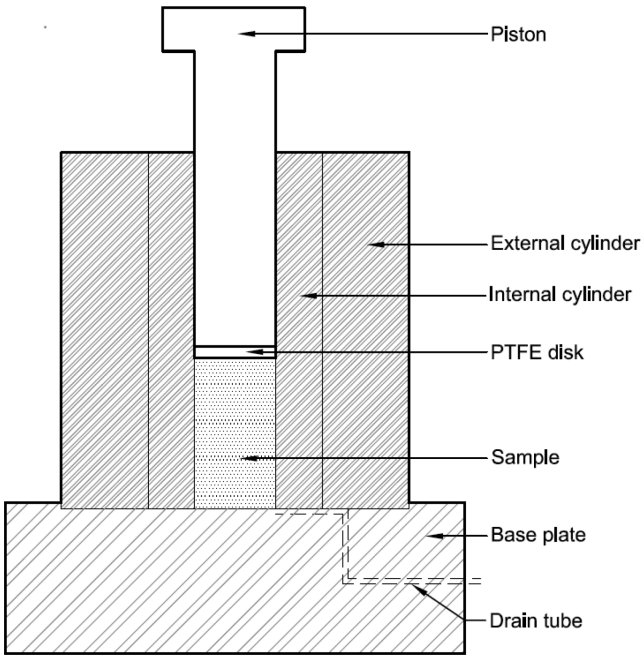

FIGURE 8 Schematic diagram of pore solution expression apparatus.

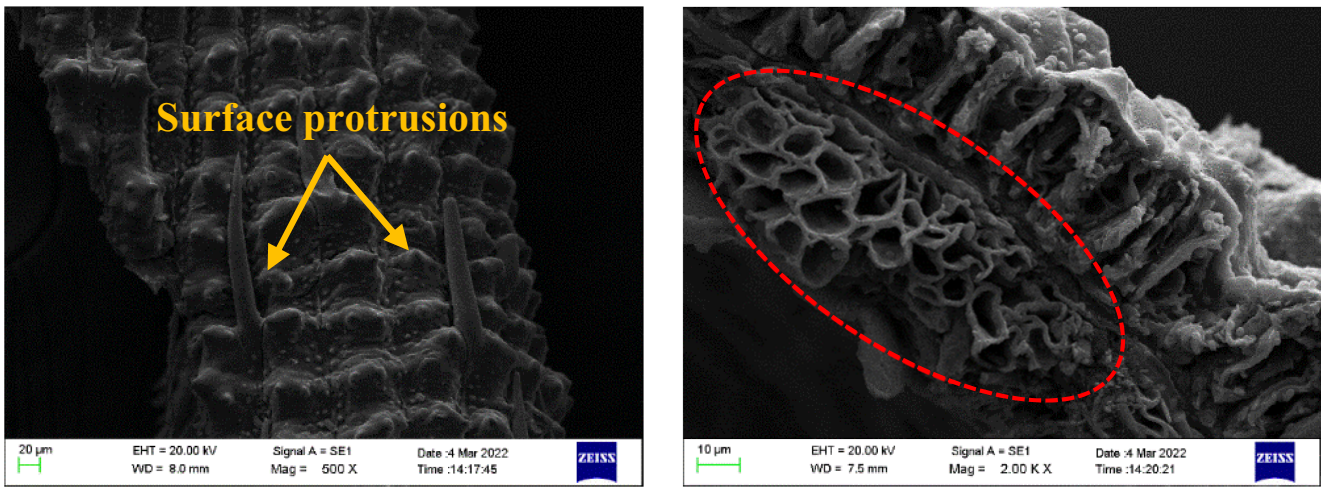

(a) (b)

FIGURE 7 SEM micrograph of: (a) surface of RB; (b) internal porous structure of RB.

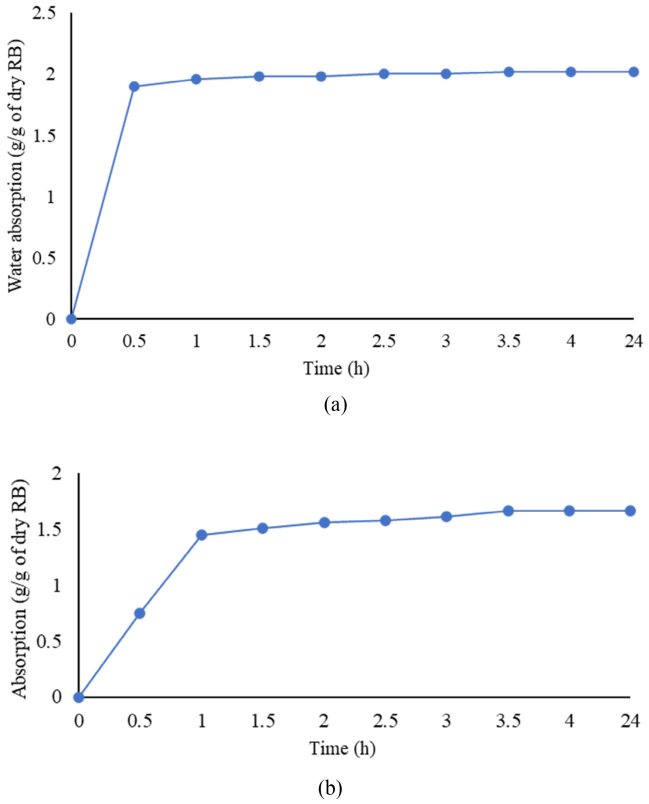

FIGURE 9 Absorption profiles of RB in: (a) water; (b) EPS-AAS.

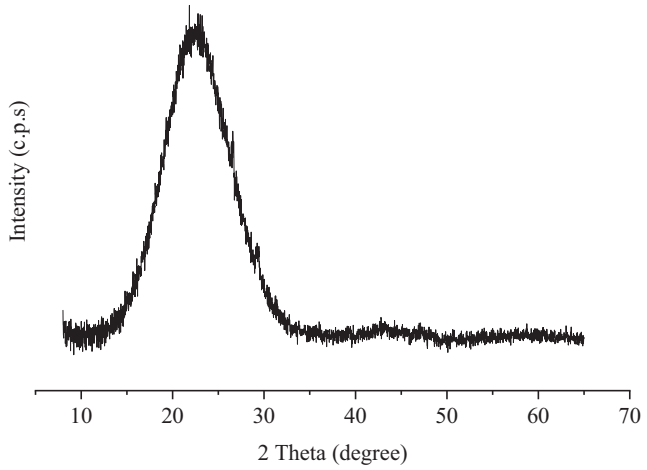

FIGURE 10 X-ray diffractogram of RB.

TABLE 2 Crystalline composition of RB.

Crystalline compound	%
Quartz	0.79
Albite	5.39
K-Feldspar	11.71
Anorthite	3.59
Illite	3.54
Calcite	2.32

the EPS-AAS instead of water. The pore solution of the AAS paste was extracted using the most widely used technique, "pore solution expression".[43,44] An AAS paste with a w/b of 0.5 was prepared (according to the procedure described in Section 2.3) and cast in cylindrical molds (50 × 100 mm). At the age of 3 days, each sample was placed inside a hollow steel cylinder where it was loosely fitted (Figure 8). A PTFE disk and the piston were placed on top of the sample. After that, the piston was loaded by placing the whole setup in a compressive strength testing machine. The pore solution was collected using a drain tube, as shown in Figure 8. A maximum pressure of 1000 MPa was applied to the piston, with a stress rate of 1.3 MPa/s. After reaching the maximum pressure of 1000 MPa, it was maintained for 15 min. The extracted pore solution was filtered through a cellulose filter (pore size 8 μm) and stored to be used for the absorption test.

The absorption of RB was calculated using Equation (1) where m_w, m_p, and m_d are the mass of the wet tea bag containing RB, the wet tea bag without RB, and dry biochar (5 g), respectively.[42,45] It was found that the absorption capacity of RB in water and EPS-AAS are 2.02 g/g of dry RB and 1.66 g/g of dry RB, respectively (Figure 9). The high absorption capacities of RB must have been caused by the cellular structure, as depicted in Figure 7b. The lower absorption capacity of RB in EPS-AAS could be due to the various ions (Si^{4+}, Al^{3+}, Na^{+}, Ca^{2+}, and OH^{-}) present in the EPS-AAS.[46]

$$\text{Absorption} = \frac{m_w - m_p - m_d}{m_d} \quad (1)$$

2.2.3 | X-ray diffraction and oxide composition

RB was well ground and sieved through a 75 μm sieve before subjecting it to XRD analysis using a BRUKER diffractometer model D2-PHASER. The obtained X-ray diffractogram of RB is shown in Figure 10. The amorphous nature of silica in RB can be identified by comparing the broad peak at $2\Theta = 22^0$ of RB with the sharp and narrow peaks of quartz at the same diffraction angle reported in the literature.[38,47] A quantitative phase analysis of the RB was conducted by interpreting the XRD analysis results using Bruker-DIFFRAC. EVA software based on the reference intensity ratio (RIR) method (based on a data file of reference intensity ratios relative to an external standard).[48,49] The results are tabulated in Table 2. It reveals that the crystalline silica content of the

TABLE 3 Oxide composition of RB.

Oxide composition (%)	RB
SiO_2	35.61
Al_2O_3	0.03
Fe_2O_3	0.02
CaO	0.33
MgO	0.14
K_2O	0.57
Na_2O	0.05
Cl	-
P_2O_5	0.1
ZnO	-
Mn_2O_3	0.06
LOI	62

RB was almost zero, further emphasizing the presence of amorphous silica in the RB. The chemical composition of RB in Table 3 shows that SiO_2 is the main oxide composition available in RB. However, as the sum of SiO_2, Al_2O_3, and Fe_2O_3 is 35.66 (<70%), RB cannot be categorized under class F pozzolans.[50] Moreover, the X-ray diffractogram and oxide composition results reveal that the RB used in this study contains a low amount of amorphous silica in comparison with rice husk ash.[51] LOI was measured by heating RB in a muffle furnace at two different temperatures. First, the RB was heated at 550°C for 5 h, and the loss on ignition at 550°C (LOI_{550}) was found to be 58%. Afterward, the RB sample was heated at 950°C for 5 h, and the loss on ignition at 950°C (LOI_{950}) was calculated to be 62%.[52,53] The organic carbon content of a material is considered to be about half of the LOI_{550} and the inorganic carbon content is $0.273 \times LOI_{950}$.[53] Thus, the approximate carbon content of RB is calculated to be 46% based on the LOI.

2.3 | Mix proportion, mixing and curing

A total of 5 mixes with different RB supplementing levels by the weight of the binder (0%, 2%, 4%, 6%, and 8%) were cast, as shown in Table 4. The Na_2O content by the weight of the binder (Na_2O-E) and the Na_2CO_3 to NaOH molar ratio were fixed at 10% and 15:10, respectively. This was done based on the previous studies and the trial experiments.[5,6,9,54] Accordingly, the required Na_2CO_3 and NaOH dosages were calculated. In order to maintain a desirable workability level in all the mixes, the w/b was selected as 0.5. The total amount of water was considered to be the water produced from NaOH and the added water. On the basis of prior investigations, the coarse aggregate to total aggregate weight ratio was maintained at 0.57.[36] The absolute volume method was used to determine the required proportions of coarse and fine aggregates.[36] The details of mixture proportions and slump values are shown in Table 4. It is worth noting that increasing biochar levels reduced the flow drastically. Similar findings have been revealed by previous researches.[9,28,42] This is attributed to the high absorption property of biochar.

Na_2CO_3 and NaOH were pre-dissolved in distilled water for 2 h prior to the concrete mixing. It was because the dissolving action was highly exothermic.[55] At first, coarse and fine aggregates were dry mixed for 2 min in a 120-L concrete mixer. Next, manually mixed slag and biochar were added to the mixer, and the mixing was continued for another 3 min. Finally, the activator solution was added and mixed for another 4 min.[56] After completing the mixing, the concrete was cast in steel molds (cube – $100 \times 100 \times 100$ mm and cylinder -150×300 mm)[57] and placed on the vibrating table for a maximum of 1-min. The samples were then put into sealed plastic bags for 3 days before demolding and subsequently cured inside the bags until testing.

2.4 | Test on hardened concrete

To determine the 28-day compressive strength, three 100-mm cubic specimens from each mix were cast. A 150×300 mm cylinder was cast for each concrete mixture, and after 28 days, it was cut into four 64-mm height discs. Three cylindrical specimens (discs) were subjected to the determination of the impact resistance. One cylindrical specimen was subjected to the drop-weight test until the first visible crack, and after that, the crack propagation, porosity, and number of voids were examined using a micro-CT scanning machine. The microstructure of the RB6 (which yielded the highest compressive strength and impact resistance) and biochar-free mix were examined through SEM.

2.4.1 | Compressive strength

The 28-day compressive strength of each AASC mix was assessed using a MATEST-3000 kN compressive strength testing apparatus with a loading rate of 0.6 MPa/s. The test was performed in accordance with BS EN 12390–3.[58] The average of 3 samples was considered the compressive strength of AASC.

TABLE 4 Mixture proportions of AASC.

Mix No	RB (%)	Slag (kg/m^3)	Biochar (kg/m^3)	Activator (kg/m^3)		Aggregates (kg/m^3)		Water (kg/m^3)	Slump (mm)
				Na_2CO_3	NaOH	Coarse	Fine		
RB0	0	450	0	57.7	14.5	951	692	225	104
RB2	2	441	9	57.7	14.5	951	692	225	101
RB4	4	432	18	57.7	14.5	951	692	225	94
RB6	6	423	27	57.7	14.5	951	692	225	72
RB8	8	414	36	57.7	14.5	951	692	225	55

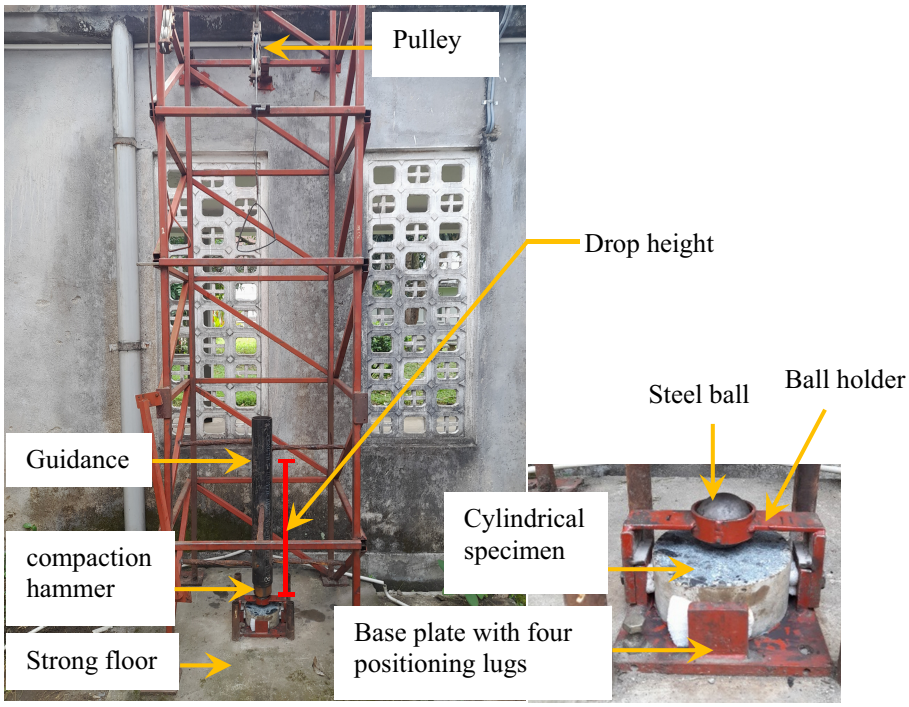

FIGURE 11 Drop-weight test apparatus.

2.4.2 | Impact resistance

This test was conducted conforming to ACI 544.[33] The drop-weight test set-up used in this study is shown in Figure 11. The cylindrical concrete specimen was placed on the steel base plate with four positioning lugs to avoid the lateral movement of the specimen during the impact test. A 63.5 –mm-diameter hardened steel ball was placed on top of the specimen. A compaction hammer weighing 4.54 kg was dropped repeatedly on top of the steel ball positioned in the center of the specimen from a fixed height of 457 mm. The number of drops required for the first visible surface crack (L_1) and for failure (L_2) needed to be recorded. Both the first visible surface crack and the failure were identified by visual observations. The first visible crack widths of the samples were measured using micro-CT scanning, and it was found that the crack widths were in the range of 90 to 300 μm. The impact energy at the initial crack (E_1) and at the failure (E_2) was calculated by the following equations:

$$E_1 = L_1 \times m \times g \times h \quad (2)$$

$$E_2 = L_2 \times m \times g \times h \quad (3)$$

where m is the mass of the compaction hammer, h is the free fall height, and g is the gravitational acceleration (9.81 m/s^2).

2.4.3 | Scanning electron microscopy (SEM) analysis

The microstructure of the AASC mixes with 0% and 6% RB was examined at the age of 28 days using FEI Quanta 200 with an accelerating voltage of 30 kV employing

secondary electrons. The samples were cut into a size of 10 mm in diameter and 10 mm in height using a diamond saw and mounted in epoxy resin. The top surface of the samples was polished manually with sandpapers (500, 800, and 1200 grid, respectively) to remove the remaining resin, then polished using a Struers polishing machine following concrete generic procedures. Subsequently, they were placed on the stubs using a double-sided conductive carbon tape and were coated with 5 – nm thick Iridium. An energy-dispersive X-ray spectroscopy (EDX) detector was employed to detect the elements, and analyzed by Aztec software.

2.4.4 | Micro-CT scanning

This test was conducted using a Ge Phoenix V tome x s CT scanning machine. The scanning voltage and current were 180 kV and 60 μA. The pixel size of the micro-CT was 88 μm. The X-ray projections were recorded with a rotation increment of 0.18° within 360°. The scanning time was approximately 5 h. The obtained scans were analyzed using VG Studio Max software to gain microstructural images of the samples. For the void analysis, two cylindrical cores with a 20 mm diameter and a 20 mm height were selected to avoid the major cracks in the specimen, and the average is reported. The voids larger than 30 μm were only considered in the void analysis due to the imaging resolution.

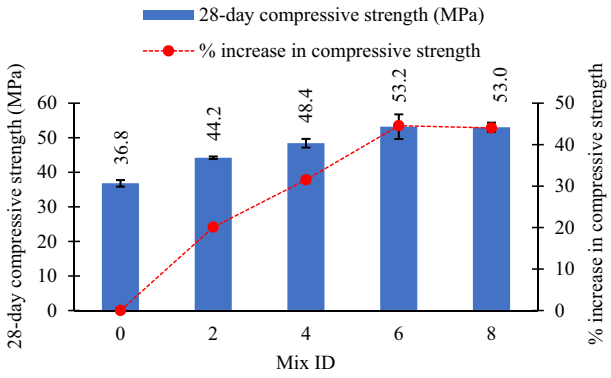

FIGURE 12 28-day compressive strength of AASC with different biochar levels.

3 | RESULTS AND DISCUSSION

3.1 | Compressive strength

Figure 12 illustrates the compressive strength variations of the AASC mixes for the different biochar levels. Increasing the biochar content by 2%, 4%, and 6% enhanced the 28-day compressive strength by 20.1%, 31.5%, and 44.6%, respectively, compared with the biochar-free concrete sample. However, the increase in biochar level from 6% to 8% showed no improvement in the compressive strength. Thus, the biochar replacement level ranging between 4% and 6% was observed to be the optimum in terms of the 28-day compressive strength. Similarly, Zeidabadi et al.[15] discovered a 20.4% increment in the 28-day compressive strength of OPC concrete with the addition of 5% RB, whereas 10% RB reduced the compressive strength. Furthermore, Egodagamage et al.[9] found that increasing the RB dosage in AAS mortar from 1% to 5% improved the 28-day compressive strength by 5.9%. The author's previous study explored the effect of RB on the hydration of alkali-activated slag mortar by conducting XRD and FTIR analyses.[9] The results revealed that the inclusion of RB in AAS does not alter the phase composition and the nature of the hydration products. In addition, a ^{29}Si NMR analysis revealed that RB increases the reaction degree of slag by 14%, which results in an enhancement in the compressive strength.[9] As RB is not a pozzolanic active material ($SiO_2 + Al_2O_3 + Fe_2O_3 < 70\%$)[47] (Table 3), it improves the compressive strength in two ways: by reducing the capillary porosity and through internal curing.[11,16,29] Porous RB (Figure 7b) tends to absorb a portion of the

TABLE 5 Drop-weight test results of AASC specimens.

	Impact numbers (L_1/L_2)				L_1	L_2	Impact energies (J)	
Mix No	Sample 1	Sample 2	Sample 3	Mean	SD	SD	First crack	Failure
RB0	171/174	185/188	186/189	181/184	8.4	8.4	3684	3745.1
RB2	178/180	185/188	190/192	184/187	6	6.1	3745.1	3806.1
RB4	377/380	392/394	386/388	385/387	7.5	7	7836.1	7876.8
RB6	510/511	516/517	518/519	515/516	4.2	4.2	10482.1	10502.5
RB8	131/132	130/131	150/151	137/138	11.3	11.3	2788.4	2808.8

Abbreviation: SD, standard deviation.

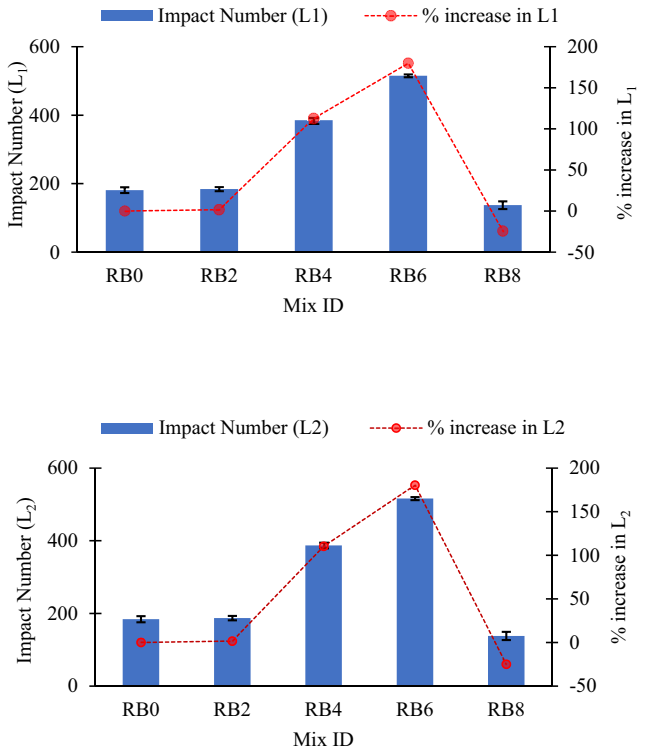

FIGURE 13 Impact numbers L_1 and L_2 of AASC with different biochar levels.

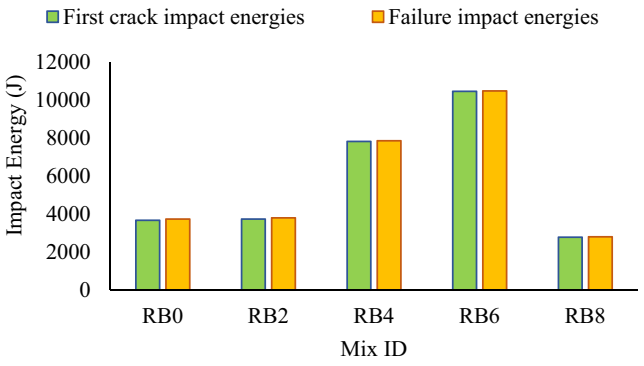

FIGURE 14 Impact energies of AASC mixes.

solution, reducing the solution/binder (S/B) ratio of the mix and resulting a significant reduction in the slump (Table 4). The reduction of the S/B lowers the evaporable water in the mix, which can create capillary pores.[59] Reducing the capillary porosity results in a denser microstructure; thus, the compressive strength is increased.[20,28] Similarly, previous studies have revealed the ability of biochar to retain the absorbed water.[11,16,17,29] Choi et al.,[17] measured the weight reduction of the mortar samples at different time intervals until 28 days, and they reported that the weight loss for the mortar mixes containing biochar over time due to moisture evaporation is less compared with the mortar mixes without biochar. This water retention property of biochar develops a moist environment, favoring the formation of the hydration products, resulting in an enhancement in the compressive strength.[9,20]

3.2 | Impact resistance

The impact resistance results of biochar-blended AASC at 28 days are listed in Table 5. It is presented in terms of the number of drops required to cause the first visible crack (L_1) and the number of drops required for the failure (L_2) of the concrete specimen. Figure 13 illustrates that increasing biochar content from 2% to 4% improved L_1 from 184 to 385 (increased by 113% compared with biochar-free sample), while further increments of biochar level up to 6% enhanced L_1 up to 515 (increased by 185% compared with the biochar-free sample). Similarly, L_2 increased from 187 to 387 and 516, when the biochar level increased from 2% to 4% and 6%, respectively. It is worth noting that when the biochar dosage was 2%, the impact resistance was almost identical to that in the biochar-free sample. Moreover, the increment of biochar content from 6% to 8% reduced both L_1 and L_2 drastically. This reduction can be due to the brittleness introduced by the RB. Akinyemi et al.[10] reported that using biochar at high dosages makes it easy to form cracks within the composite due to the brittleness of the biochar. Generally, less ductility, high compressive strength, and poor capacity to resist impact loads are features of brittle materials.[60] Therefore, the low impact resistance (Figure 13) and high compressive strength (Figure 12) of the RB8 illustrate the enhanced brittleness of the composite. Figure 14 shows the change in impact energies of the AASC mixes with the increment of the biochar dosage. Based on the results, an optimum replacement level of RB is recommended, ranging between 4% and 6%, to achieve improved impact resistance. As anticipated, this increment in impact resistance is due to the densification effect caused by RB on the AASC. Similar explanations have been reported for different supplements in concrete, such as silica fume.[24–26]

3.3 | Failure patterns

Figure 15 illustrates the failure patterns of the AASC samples subjected to the drop-weight test. All five mixes could not sustain more than three impacts after the initial cracking, and that indicates the brittle nature of the AASC material. With the increasing biochar dosage from 0% to 8%, the samples demonstrated an increasing trend

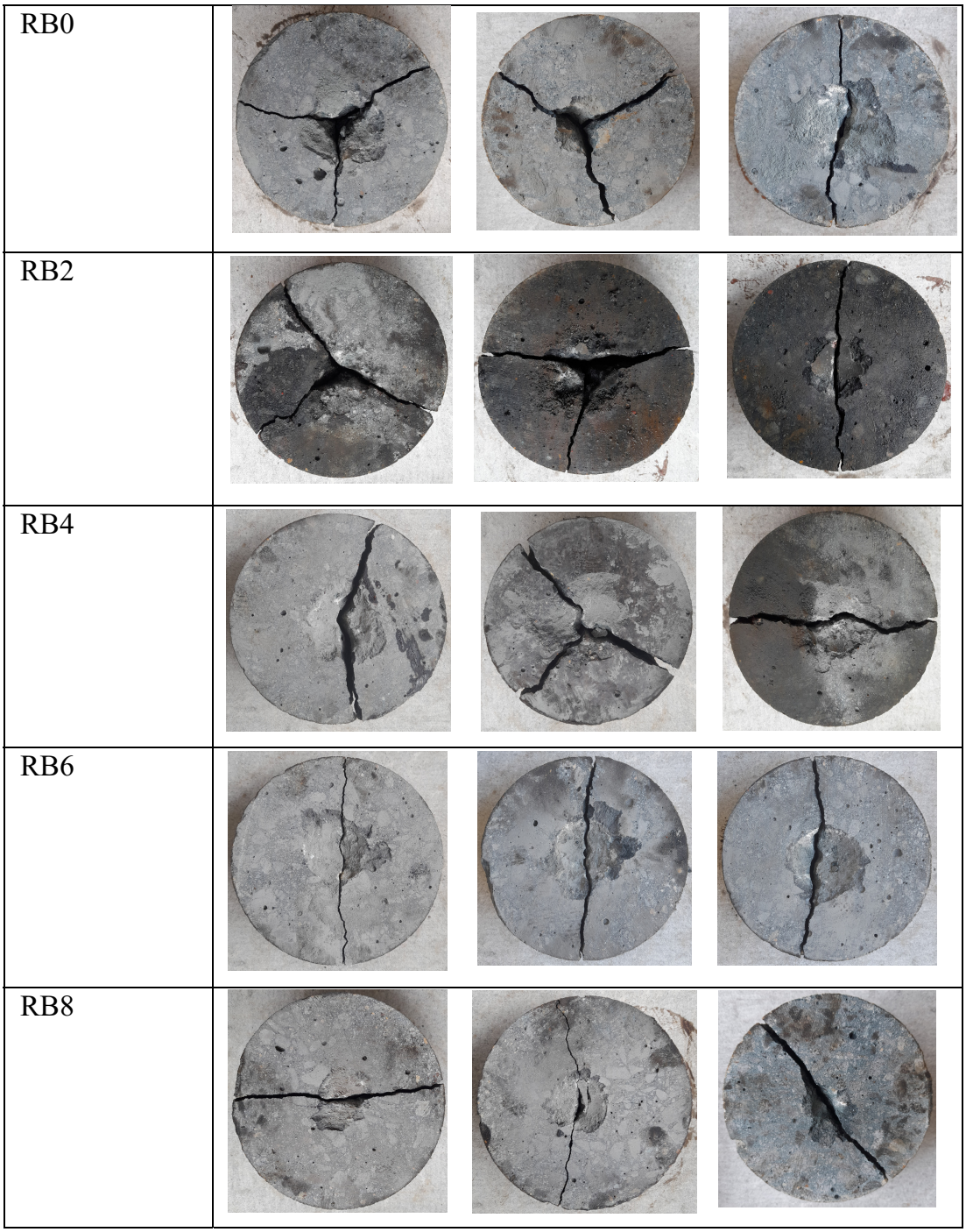

FIGURE 15 Failure patterns of AASC mixes against drop weight impact.

to fracture along a single diagonal crack. This indicates an increment in the brittleness of the composite due to the increasing biochar content.[10,61] Also, it is agreeable with the low impact resistance results of the RB8 (Figure 13). Similarly, previous studies have demonstrated that when the brittleness of the material is reduced, the failure mechanism is transferred from a single diagonal crack to multiple diagonal cracks.[25,62–64]

3.4 | Microstructure: SEM Analysis

The microstructural properties of the two AASC samples with 6% RB (which was given the highest compressive and impact resistance) and 0% RB are illustrated in Figure 16. RB6 showed a dense microstructure with less micro pores in comparison to the control mix. Moreover, a continuous formation of the C-A-S-H gel with less

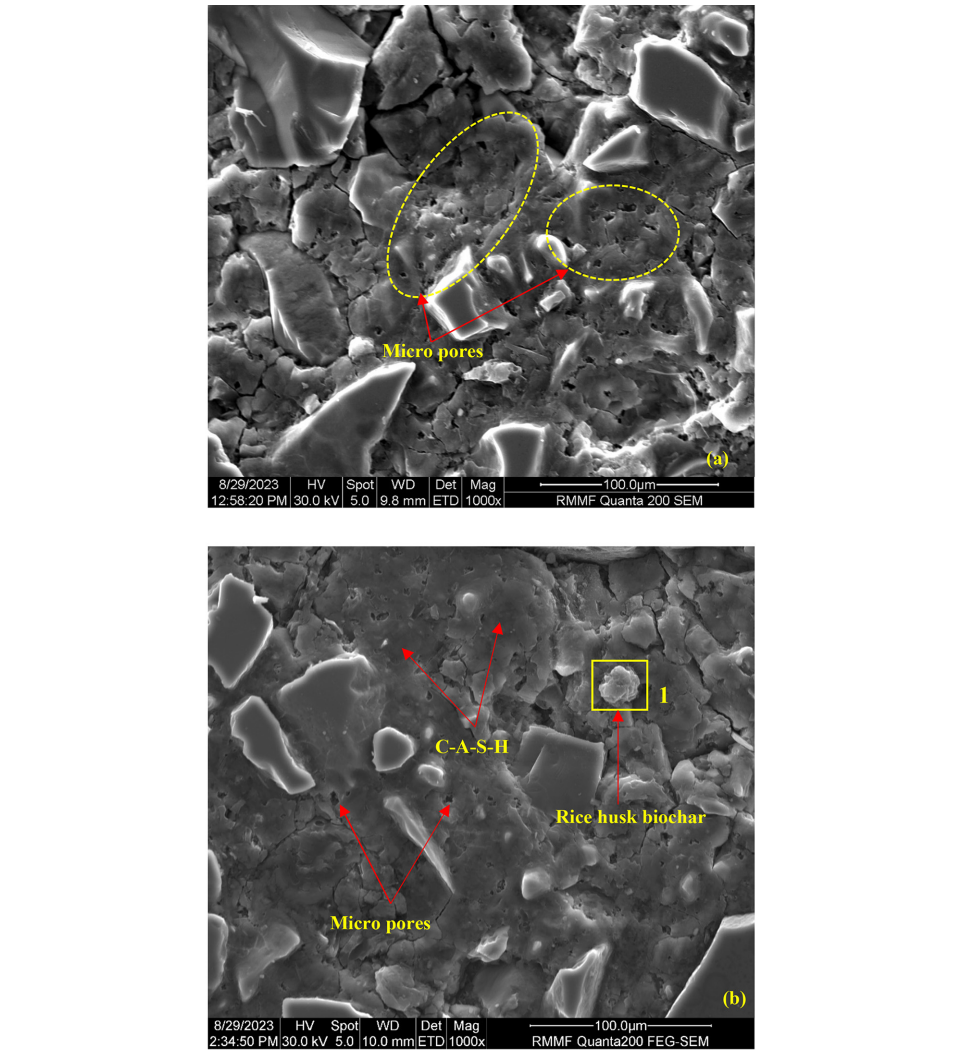

FIGURE 16 SEM/EDX image of: (a) RB0; (b) RB6.

disturbances was visible in the RB6 relative to the control mix. This dense microstructure resulted in an observed enhancement in the compressive strength (Figure 12) and impact resistance (Figure 13). Furthermore, an SEM/EDX analysis was conducted on the RB6 sample to examine the RB particles in the matrix. RB particles could be identified with a high C content (65.6%), which is an inherent characteristic of biochar.[11,13,16,38,47,65]

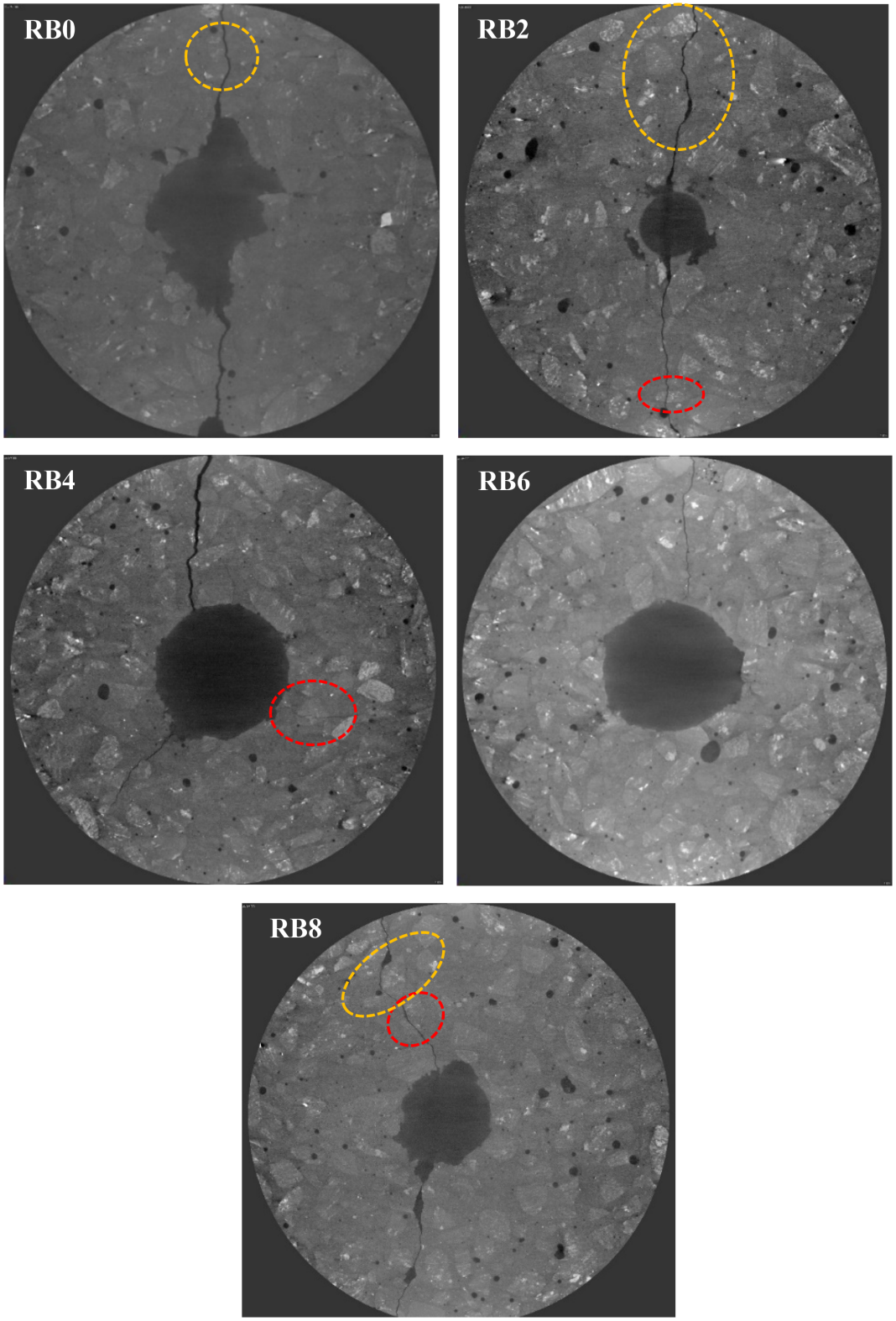

FIGURE 17 Micro-CT scanning images of AASC samples subjected to drop impact test.

Similarly, the approximate C content of RB calculated based on the LOI was as high as 46%. When comparing the minor elements detected on the RB surface with its initial chemical composition (Table 3), the increased Na content could be due to the retained alkaline activator by the RB.

3.5 | Characterization of crack propagation by micro-CT

Figure 17 illustrates the impact surface of the five AASC samples (with different biochar levels) that were subjected to the drop impact test. It is visible that the cracks

TABLE 6 Porosity and number of voids larger than 30 μm in the AASC mixes.

Mix No	Porosity (%)	Number of voids
RB0	0.24	15,294
RB2	4.00	183,147
RB4	3.37	154,301
RB6	2.28	104,394
RB8	3.17	145,144

are strongly curved around the aggregates (highlighted with yellow dotted lines). Moreover, the majority of the cracks propagated close to the aggregates in the interfacial transition zones (ITZ), which is the weakest phase in concrete. However, occasionally, cracks propagated through the aggregates as well (highlighted with red dotted lines). It could be observed that the crack propagation is almost similar in all the samples. Thus, RB has not caused a significant effect on the crack propagation of the AASC.

3.6 | Void structure analysis by micro-CT

The total porosity and total number of voids larger than 30 μm are tabulated in Table 6. The porosity of the AASC mixes with RB was higher than that of the AASC mixes without RB. A similar observation has been reported by Prabahar et al.[42] This is due to the presence of voids in the biochar. However, a declining trend of porosity was observed with the increment of the RB percentage from 2% to 4% and 6%. This reduction in porosity is due to the densification effect caused by RB on the AASC. The decline in porosity with the inclusion of RB up to 6% was well in agreement with the compressive strength (Figure 12) and impact resistance results (Figure 13). As expected, the porosity increased from 2.28% to 3.17%, with the increase of the RB level from 6% to 8%. A similar trend was observed in the number of voids, and the results agreed with the porosity results.

4 | CONCLUSIONS AND FUTURE WORK

This study explored the influences of biochar on the strength and impact resistance of alkali-activated slag concrete (AASC). The concrete was supplemented with different dosages of rice husk biochar -RB (0%, 2%, 4%, 6%, and 8%) that were pyrolyzed at 500°C. A combination of Na_2CO_3 and NaOH (Na_2CO_3: NaOH molar ratio was 15:10) was used as the alkaline activator, and the Na_2O content was 10% of the weight of the binder. Based on the findings, the following conclusions can be drawn:

1. The supplementation of RB at 2%, 4%, and 6% in AASC caused 28-day compressive strength enhancements of 20.1%, 31.5%, and 44.6%, respectively, in contrast to the control mix. This was due to the biochar's ability to reduce the capillary porosity of the mix and impose an internal curing effect. However, the strength enhancement was not pronounced between 6% and 8% RB scenarios.
2. The slump of the concrete was reduced with the increasing biochar content due to the high absorption characteristic of porous biochar.
3. The supplementation of biochar to 6% had a significant influence on the impact resistance in AASC. The number of drops required at the drop hammer test for the first visible crack (L_1) and the failure (L_2) increased in the RB 6% mix by 185% and 175%, respectively, as opposed to the control mix. These improvements were attributed to the ability of biochar to densify the microstructure (Figure 16). Meanwhile, when the RB dosage was altered from 6% to 8%, the impact resistance drastically reduced due to the fact that the brittleness of the composite escalated at the high RB level. This particular judgment was evidenced by the increasing trend of the AASC samples to fracture along a single diagonal crack upon impact, with the increasing biochar dosage from 0% to 8% (Figure 15).
4. Micro-CT scanning results revealed that RB did not cause a significant effect on the crack propagation of the AASC.
5. High impact resistance is ideal for concrete structures exposed to impacts such as vehicular collisions, the falling of masses (e.g., road barriers, rock fall protection walls), and accidental impacts due to explosions. Hence, full-scale testing of the impact resistance of AASC is vital and a recommendable matter for future work. Similarly, recycled expanded polystyrene (EPS) is considered a good supplement in concrete to reach high energy absorption; however, the compressive strength is rather compromised. In that scenario, it could be interesting to explore the potential of the dual blending of biochar and EPS in AASC to develop a strong and impact-resilient product.

ACKNOWLEDGMENTS

This project is funded as part of the CRC-P on upcycling solutions for hazardous claddings and co-mingled waste (CRCPEIGHT000084). The assistance provided by Siam City Cement (Lanka) Limited and the Materials/Environmental Laboratories and Engineering Workshop of the Civil Engineering Department of the University of

Peradeniya is also greatly acknowledged. Open access publishing facilitated by RMIT University, as part of the Wiley - RMIT University agreement via the Council of Australian University Librarians.

CONFLICT OF INTEREST STATEMENT

The authors declare that they have no conflict of interest.

DATA AVAILABILITY STATEMENT

The research data are included within the article, and further data are available from the first and corresponding author upon request.

ORCID

Harshani Egodagamage https://orcid.org/0009-0009-2951-6469
Hiran Yapa https://orcid.org/0000-0002-7213-5276
Samith Buddika https://orcid.org/0000-0002-4592-0738
Thomas Loh https://orcid.org/0000-0002-1996-346X
Satheeskumar Navaratnam https://orcid.org/0000-0001-7772-4531
Yulin Patrisia https://orcid.org/0000-0002-9254-3306
Kate Nguyen https://orcid.org/0000-0002-1825-4127

REFERENCES

1. Abdalqader AF, Jin F, Al-Tabbaa A. Development of greener alkali-activated cement: utilisation of sodium carbonate for activating slag and fly ash mixtures. J Clean Prod. 2016;113:66–75.
2. Awoyera P, Adesina A. A critical review on application of alkali activated slag as a sustainable composite binder. Case Stud Constr Mater. 2019;11:e00268.
3. Yang K-H, Song J-K, Song K-I. Assessment of CO2 reduction of alkali-activated concrete. J Clean Prod. 2013;39:265–72.
4. Gao X, Yao X, Yang T, Zhou S, Wei H, Zhang Z. Calcium carbide residue as auxiliary activator for one-part sodium carbonate-activated slag cements: compressive strength, phase assemblage and environmental benefits. Construct Build Mater. 2021;308:125015.
5. Jiao Z, Wang Y, Zheng W, Huang W. Effect of dosage of sodium carbonate on the strength and drying shrinkage of sodium hydroxide based alkali-activated slag paste. Construct Build Mater. 2018;179:11–24.
6. Zhang J, Tan H, Cai L, He X, Yang W, Liu X. Ultra-fine slag activated by sodium carbonate at ambient temperature. Construct Build Mater. 2020;264:120695.
7. Rashad AM, Bai Y, Basheer PA, Milestone NB, Collier NC. Hydration and properties of sodium sulfate activated slag. Cem Concr Compos. 2013;37:20–9.
8. Tan H, Deng X, He X, Zhang J, Zhang X, Su Y, et al. Compressive strength and hydration process of wet-grinded granulated blast-furnace slag activated by sodium sulfate and sodium carbonate. Cem Concr Compos. 2019;97:387–98.
9. Egodagamage H, Yapa H, Buddika HS, Navaratnam S, Nguyen K. Effective use of biochar as an additive for alkali-activated slag mortar production. Construct Build Mater. 2022;370:130487.
10. Akinyemi BA, Adesina A. Recent advancements in the use of biochar for cementitious applications: a review. J Build Eng. 2020;32:101705.
11. Gupta S, Kua HW, Low CY. Use of biochar as carbon sequestering additive in cement mortar. Cem Concr Compos. 2018;87:110–29.
12. Gupta S, Kashani A, Mahmood AH, Han T. Carbon sequestration in cementitious composites using biochar and fly ash – effect on mechanical and durability properties. Construct Build Mater. 2021;291:123363.
13. Praneeth S, Guo R, Wang T, Dubey BK, Sarmah AK. Accelerated carbonation of biochar reinforced cement-fly ash composites: enhancing and sequestering CO2 in building materials. Construct Build Mater. 2020;244:118363.
14. Gupta S, Kua HW. Carbonaceous micro-filler for cement: effect of particle size and dosage of biochar on fresh and hardened properties of cement mortar. Sci Total Environ. 2019;662:952–62.
15. Zeidabadi ZA, Bakhtiari S, Abbaslou H, Ghanizadeh AR. Synthesis, characterization and evaluation of biochar from agricultural waste biomass for use in building materials. Construct Build Mater. 2018;181:301–8.
16. Gupta S, Kua HW, Pang SD. Biochar-mortar composite: manufacturing, evaluation of physical properties and economic viability. Construct Build Mater. 2018;167:874–89.
17. Choi WC, Yun HD, Lee JY. Mechanical properties of mortar containing bio-char from pyrolysis. J Korea Inst Struct Mainten Inspec. 2012;16:67–74.
18. Leng L, Xiong Q, Yang L, Li H, Zhou Y, Zhang W, et al. An overview on engineering the surface area and porosity of biochar. Sci Total Environ. 2021;763:144204.
19. Maljaee H, Madadi R, Paiva H, Tarelho L, Ferreira VM. Incorporation of biochar in cementitious materials: a roadmap of biochar selection. Construct Build Mater. 2021;283:122757.
20. Chen X, Li J, Xue Q, Huang X, Liu L, Poon CS. Sludge biochar as a green additive in cement-based composites: mechanical properties and hydration kinetics. Construct Build Mater. 2020;262:120723.
21. Yu R, Spiesz P, Brouwers H. Energy absorption capacity of a sustainable ultra-high performance fibre reinforced concrete (UHPFRC) in quasi-static mode and under high velocity projectile impact. Cem Concr Compos. 2016;68:109–22.
22. Yu R, Beers LV, Spiesz P, Brouwers H. Impact resistance of a sustainable ultra-high performance fibre reinforced concrete (UHPFRC) under pendulum impact loadings. Construct Build Mater. 2016;107:203–15.
23. Kangning L, ChunYuan J, Tianyi Y, Dingqiang F, Juntao K, Rui Y. Enhancement of impact resistance for low water/binder cementitious composites (LWBCC) based on porous aggregate: from the perspective of macroscopic and microscopic. Construct Build Mater. 2023;376:130952.
24. Gupta T, Sharma RK, Chaudhary S. Impact resistance of concrete containing waste rubber fiber and silica fume. Int J Impact Eng. 2015;83:76–87.
25. Nili M, Afroughsabet V. Combined effect of silica fume and steel fibers on the impact resistance and mechanical properties of concrete. Int J Impact Eng. 2010;37:879–86.
26. Ameri F, Brito JD, Madhkhan M, Taheri RA. Steel fibre-reinforced high-strength concrete incorporating copper slag:

mechanical, gamma-ray shielding, impact resistance, and microstructural characteristics. J Build Eng. 2020;29:101118.
27. Jia Y, Li H, He X, Li P, Wang Z. Effect of biochar from municipal solid waste on mechanical and freeze–thaw properties of concrete. Construct Build Mater. 2023;368:130374.
28. Gupta S, Kua HW. Effect of water entrainment by pre-soaked biochar particles on strength and permeability of cement mortar. Construct Build Mater. 2018;159:107–25.
29. Gupta S, Kua HW, Koh HJ. Application of biochar fromfood and wood waste as green admixture for cement mortar. Sci Total Environ. 2018;619-620:419–35.
30. Nis A, Eren NA, Çevik A. Effects of nanosilica and steel fibers on the impact resistance of slag based self-compacting alkali-activated concrete. Ceram Int. 2021;47:23905–18.
31. Xu Y, Xing G, Zhao J, Zhang Y. The effect of polypropylene fiber with different length and dosage on the performance of alkali-activated slag mortar. Construct Build Mater. 2021;307: 124978.
32. Abubakr A, Soliman A, Diab S. Effect of activator nature on the impact behaviour of alkali-activated slag mortar. Construct Build Mater. 2020;257:119531.
33. ACI 544.2R. Measurement of properties of fiber reinforced concrete. Farmington Hills, MI: American Concrete Institute; 1999.
34. Wang Q, Ding Y, Zhang Y, Castro C. Effect of macro polypropylene fiber and basalt fiber on impact resistance of basalt fiber-reinforced polymer-reinforced concrete. Structural Concrete. 2021;22:503–15.
35. Haruna SI, Zhu H, Shao J. Experimental study, modeling, and reliability analysis of impact resistance of micro steel fiber-reinforced concrete modified with nano silica. Structural Concrete. 2022;23:1659–74.
36. Nanayakkara O, Gunasekara C, Sandanayake M, Law DW, Nguyen K, Xia J, et al. Alkali activated slag concrete incorporating recycled aggregate concrete: long term performance and sustainability aspect. Construct Build Mater. 2021;271:121512.
37. ASTM Standard C33. Standard specification for concrete aggragates. West Conshohocken, PA: ASTM Int; 2009.
38. Gupta S, Kua HW. Application of rice husk biochar as filler in cenosphere modified mortar: preparation, characterization and performance under elevated temperature. Construct Build Mater. 2020;253:119083.
39. Tan K, Pang X, Qin Y, Wang J. Properties of cement mortar containing pulverized biochar pyrolyzed at different temperatures. Construct Build Mater. 2020;263:120616.
40. Zielinska A, Oleszczuk P, Charmas B, Skubiszewska-Zieba J, Pasieczna-Patkowska S. Effect of sewage sludge properties on the biochar characteristic. J Anal Appl Pyrolysis. 2015;112: 201–13.
41. Fidel RB, Laird DA, Thompson ML, Lawrinenko M. Characterization and quantification of biochar alkalinity. Chemosphere. 2017;167:367–73.
42. Prabahar J, Vafaei B, Baffoe E, Ghahremaninezhad A. The effect of biochar on the properties of alkali-activated slag pastes. Constr Mater. 2022;2:1–14.
43. Buckley LJ, Carter MA, Wilson MA, Scantlebury JD. Methods of obtaining pore solution from cement pastes and mortars for chloride analysis. Cem Concr Res. 2007;37: 1544–50.
44. Liu X, Niu D, Li X, Lv Y, Fu Q. Pore solution pH for the corrosion initiation of Rebars embedded in concrete under a long-term natural carbonation reaction. Appl Sci. 2018;8:128.
45. Farzanian K, Vafaei B, Ghahremaninezhad A. The influence of the chemical composition of hydrogels on their behavior in cementitious materials. Mater Struct. 2021;54:244.
46. Zuo Y, Nedeljković M, Ye G. Pore solution composition of alkali-activated slag/fly ash pastes. Cem Concr Res. 2019;115: 230–50.
47. Gupta S, Muthukrishnan S, Kua HW. Comparing influence of inert biochar and silica rich biochar on cement mortar – hydration kinetics and durability under chloride and sulfate environment. Construct Build Mater. 2021;268:121142.
48. Zhou X, Liu D, Bu H, Deng L, Liu H, Yuan P, et al. XRD-based quantitative analysis of clay minerals using reference intensity ratios, mineral intensity factors, Rietveld, and full pattern summation methods: a critical review. Solid Earth Sciences. 2018;3: 16–29.
49. Hubbard CR, Evans EH. The reference intensity ratio, I/Ic, for computer simulated powder patterns. J Appl Cryst. 1976;9: 169–74.
50. ASTM. Standard specification for coal Fly ash and raw or calcined natural Pozzolan for use in concrete. West Conshohocken, PA: ASTM; 2019.
51. Hwang C-L, Huynh T-P. Effect of alkali-activator and rice husk ash content on strength development of fly ash and residual rice husk ash-based geopolymers. Construct Build Mater. 2015; 101:1–9.
52. Raya-Moreno I, Cañizares R, Domene X, Carabassa V, Alcañiz JM. Comparing current chemical methods to assess biochar organic carbon in a Mediterranean agricultural soil amended with two different biochars. Sci Total Environ. 2017; 598:604–18.
53. Santisteban JI, Mediavilla R, Lo´ E, Pez-Pamo CJD, Zapata MBR, Garcı'a MJG, et al. Loss on ignition: a qualitative or quantitative method for organic matter and carbonate mineral content in sediments? J Paleo. 2004;32:287–99.
54. Akturk B, Nayak S, Asce S, Das S, Asce A, Kizilkanat AB. Microstructure and strength development of sodium carbonate–activated blast furnace slags. J Mater Civ Eng. 2019; 31:11.
55. Akturk B, Kizilkanat AB. Improvement of durability and drying shrinkage of sodium carbonate activated slag through the incorporation of calcium hydroxide and sodium hydroxide. Construct Build Mater. 2020;243:118260.
56. Thunuguntla CS, Rao TDG. Effect of mix design parameters on mechanical and durability properties of alkali activated slag concrete. Construct Build Mater. 2018;193:173–88.
57. T. B. S. Institution. Testing hardened concrete: part 1: shape, dimensions and other requi rements for specimens and moulds. *BS EN 12390-1*. 2012.
58. E. 12390-3. Testing hardened concrete – part 3: compressive strength of test specimens. *EN 12390-3*. 2001.
59. Najimi M, Ghafoori N, Sharbaf M. Alkali-activated natural pozzolan/slag mortars: a parametric study. Construct Build Mater. 2018;164:625–43.
60. Zhang H. The basic properties of building materials. Building materials in civil engineering. Sawston, CA: Woodhead Publishing; 2011. p. 7–28.

61. Ali D, Agarwal R, Hanifa M, Rawat P, Paswan R, Rai D, et al. Thermo-physical properties and microstructural behaviour of biochar-incorporated cementitious material. J Build Eng. 2023; 64:105695.
62. Haridharan MK, Matheswaran S, Murali G, Abid SR, Fediuk R, Amran YHM, et al. Impact response of two-layered grouted aggregate fibrous concrete composite under falling mass impact. Construct Build Mater. 2020;263:120628.
63. Abirami T, Loganaganandan M, Murali G, Fediuk R, Sreekrishna RV, Vignesh T, et al. Experimental research on impact response of novel steel fibrous concretes under falling mass impact. Construct Build Mater. 2019;222:447–57.
64. Rahmani T, Kiani B, Shekarchi M, Safari A. Statistical and experimental analysis on the behavior of fiber reinforced concretes subjected to drop weight test. Construct Build Mater. 2012;37:360–9.
65. Navaratnam S, Wijaya H, Rajeev P, Mendis P, Nguyen K. Residual stress-strain relationship for the biochar-based mortar after exposure to elevated temperature. Case Stud Constr Mater. 2021;14:e00540.

AUTHOR BIOGRAPHIES

Harshani Egodagamage - PhD Student, School of Engineering, RMIT University, Melbourne, Australia. Email: s3892528@student.rmit.edu.au.

Hiran Yapa - PhD, Professor, Department of Civil Engineering, Faculty of Engineering, University of Peradeniya, Sri Lanka. Email: hdy@eng.pdn.ac.lk.

Samith Buddika - PhD, Senior Lecturer, Department of Civil Engineering, Faculty of Engineering, University of Peradeniya, Sri Lanka. Email: samithbuddika@eng.pdn.ac.lk.

Thomas Loh - PhD, School of Engineering, RMIT University, Melbourne, Australia. Email: thomas.loh@rmit.edu.au.

Satheeskumar Navaratnam - PhD, Lecturer, School of Engineering, RMIT University, Melbourne, Australia. Email: sathees.nava@rmit.edu.au.

Yulin Patrisia - PhD, School of Engineering, RMIT University, Melbourne, Australia. Email: yulin.patrisia@rmit.edu.au.

Kate Nguyen - PhD, Associate Professor, Leader of Innovative Fire and Facade Engineering Group, School of Engineering, RMIT University, Melbourne, Australia. Email: kate.nguyen@rmit.edu.au.

How to cite this article: Egodagamage H, Yapa H, Buddika S, Loh T, Navaratnam S, Patrisia Y, et al. Enhancement of impact resistance of alkali-activated slag concrete through biochar supplementation. Structural Concrete. 2024;25(5): 3630–47. https://doi.org/10.1002/suco.202300469